Reconstruction of the SiO_2 structure damaged by low-energy Ar-implanted ions

B. Garrido,[a] J. Samitier, S. Bota, and J. A. Moreno
EME, Departament de Física Aplicada i Electrònica, Universitat de Barcelona, Diagonal 645-647, 08028 Barcelona, Spain

J. Montserrat
Centre Nacional de Microelectrònica, CNM-CSIC, Campus Universitat Autònoma de Barcelona, 08193 Bellaterra, Spain

J. R. Morante
EME, Department de Fisica Aplicada i Electrònica, Universitat de Barcelona, Diagonal 645-647, 08028 Barcelona, Spain

(Received 1 March 1996; accepted for publication 23 September 1996)

The damage created in SiO_2 layers by low-energy Ar ions (130 keV) and the reconstruction of the structure after various annealing steps have been characterized as a function of the implantation dose. Quantitative determinations of the damage produced have been performed from infrared spectroscopy. We show that two dose thresholds for damage are encountered: At 10^{14} cm^{-2} damage saturates and for doses above 10^{17} cm^{-2} sputtering effects dominate. Annealing at high temperatures (1100 °C) restores the structure of the initial nonimplanted oxide only for doses below the second threshold, although some disorder remains. Electroluminescence measurements show that annealing is able to eliminate electrically active defects. For implantation doses greater than 10^{17} cm^{-2}, annealing is unable to restore the structure completely as sputtering effects create a depleted oxygen layer at the surface and substoichiometric defects appear. The presence of microcavities created by the Ar atoms at such high doses may affect the annealing behavior. © *1997 American Institute of Physics.* [S0021-8979(97)02001-X]

I. INTRODUCTION

Many studies have analyzed the effects of radiation damage in SiO_2/Si systems[1–6] as ion bombardment and other types of radiation are applied during their manufacture. Moreover, several techniques for surface analysis use ion beams to measure physical and structural properties, such as secondary-ion-mass spectroscopy (SIMS), x-ray photoelectron spectroscopy (XPS), Auger spectroscopy, etc. These radiation sources affect the structure, properties, and reliability of the Si/SiO_2 system. Furthermore, doping through oxide masks and modifications of SiO_2 etch rates are also undertaken by using ion implantation techniques. Therefore, there is an intrinsic interest in the basic and applied research related to the modifications of the structure in amorphous solids created by ion beams. In this framework, low-dose ion implantation with Ar causes damage and disorder in the SiO_2 layer, but without changing the composition of the layer, as Ar atoms cannot form stable bonds with the silicon or oxygen atoms.

It is, therefore, essential to understand how the SiO_2 structure is modified after implantation, what kind of defects are created and what annealing treatments can do to restore the structure. The structural damage produced in the amorphous network of silicon oxide as a consequence of ion implantation is characterized by strained and broken bonds, distortion of silicon tetrahedra, densification, departure from local stoichiometry, and, in the case of irradiation with fast heavy ions, plastic flow phenomena.

We have previously reported[5,7] that the damage produced by Ar ions in SiO_2 layers increases with the implantation dose, for low doses; however, for doses higher than 10^{14} cm^{-2} damage saturates. Various authors have reported similar behavior when other ions are implanted into silica. This has been shown to be almost independent of the type of ion implanted.[2–10] Moreover, Ar-implanted oxide layers have presented a degree of densification after implantation.[5,7,11] Densification is accompanied by other structural modifications, such as Si—O bond straining and bond breaking, as a consequence of atom displacement from positions of equilibrium. Indeed, Devine[4] has reported that the creation of defects is greatly enhanced in densified amorphous SiO_2, as strained Si—O bonds act as precursors for both oxygen vacancy and nonbridging oxygen defects. Infrared spectra give clear evidence of the reduction in the mean Si—O—Si bond angle as well as of the presence of low-frequency vibrations coming from Si—O nonbridging oxygen bonds.[5] The XPS analysis of the local environments of silicon atoms performed by the authors corroborated the presence of dangling bonds and allowed their distribution as a function of the damage created to be calculated.[5] Therefore, one expects radiation damage to induce stable oxygen atom displacements in the a-SiO_2 network.

In this framework, here we analyze the damage in SiO_2 following very high Ar implantation doses ($>10^{17}$ cm^{-2}), well above the threshold for damage saturation. We also report the experimental annealing experiments performed at different temperatures with the aim of restoring the structure of the a-SiO_2 network.

[a]Electronic mail: blas@iris1.fae.ub.es

 0021-8979/97/81(1)/126/9/$10.00

II. EXPERIMENTAL PROCEDURE

The substrates used were ⟨100⟩ *n*-type, phosphorus-doped (1.0×10^{15} cm^{-3}) silicon wafers, with resistivity between 3 and 5 Ω cm. The oxide layers were grown by wet oxidation at 950 °C. The thickness of these layers before the implantation and the annealing processes was around 2500 Å as measured by ellipsometry. In measuring the oxide thickness it is important that the implanted ions do not reach the silicon substrate. In previous studies we analyzed as-implanted samples up to doses near the threshold for damage saturation (10^{14}–10^{15} cm^{-2}).[5,7,11] Here, we increased the range of doses up to 3.2×10^{17} cm^{-2}, and we performed rapid thermal annealing (RTA) in N_2 and O_2 for all the samples, at different temperatures (from 400 to 1100 °C) and duration times (from 1 s to 1 min).

The energy of Ar ions (130 keV) was chosen so that the maximum distribution of the implanted ions was in the middle of the layer (this was previously calculated by computer simulation). The implantation was performed by using an Eaton Nova 4206 implanter; cooling and a low-beam current were used to avoid heating.

For the Fourier transform infrared spectroscopy (FTIR) measurements, the SiO_2 films on the reverse side of the substrate were etched off in order to prevent infrared absorption by the nonimplanted film. Both reflection and transmission operation modes were used in a BOMEM DA3 spectrometer. Infrared spectra were measured for all the samples in the midinfrared range (4000–400 cm^{-1}) at a resolution of 2 cm^{-1}. Raw spectra were appropriately rationed to a bare silicon spectrum.

The electroluminescence (EL) measurements were performed with an alternative technique which is based on the use of an electrolyte–oxide–semiconductor (EOS) system, to carry out a controlled injection and heating of electrons in SiO_2 films depending on the applied electric field. This technique allowed us to perform defect characterization without the need to deposit any metal or polycrystalline silicon contact. In contrast with other techniques, EL gives information of electrically active defects in the oxide. Further details of this last technique are explained in the literature.[12] Furthermore, some etching-rate measurements in a buffered HF mixture were selectively performed in some of the samples.

III. INFRARED AND ELLIPSOMETRY RESULTS

A. Samples as implanted with Ar

The infrared spectra of the implanted samples show a strong modification of the SiO_2 stretching band. This is the most intense band of the SiO_2 infrared spectrum, and in transmission at normal incidence it is composed of two transverse optic (TO) vibrational modes, the TO_3 or asymmetric stretching mode and the TO_4 or symmetric stretching mode, which in nonimplanted thermal oxides are centered around 1080 and 1200 cm^{-1}, respectively.[13,14] After the implantation, the whole stretching band becomes shifted markedly toward lower wave numbers, it becomes broader and both its intensity and area decrease. Figure 1 shows the absorption spectra of SiO_2 after implantation doses ranging from 3.2×10^{12} to 3.2×10^{17} cm^{-2}. The shift and broadening of the stretching band increases with implantation dose, but reaches a saturation regime after a dose threshold of 10^{14} cm^{-2}, which corresponds to a nuclear deposited energy of 4.6×10^{23} eV/cm^3, in agreement with previous works.[2,6] This energy is only slightly higher than the Si—O bond energy density, which is 3.8 eV/bond or 3.4×10^{23} eV/cm^3, which suggests that structural damage efficiency for nuclear collisions is higher than for electronic losses. This assumption is corroborated by the amount of energy required to reach saturation when using MeV proton or electron irradiation—values around or higher than 10^{26} eV/cm^3.[9,10]

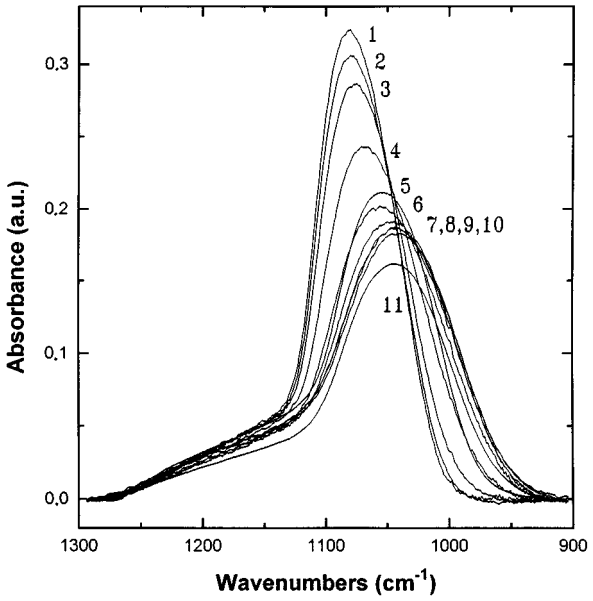

FIG. 1. Infrared-absorbance spectra of the implanted samples for different doses (in cm^{-2}) in the region of the TO_3 and TO_4 modes. 1: Reference nonimplanted sample; 2: 3.2×10^{12}; 3: 1.0×10^{13}; 4: 3.2×10^{13}; 5: 1.0×10^{14}; 6: 3.2×10^{14}; 7: 3.2×10^{15}; 8: 1.0×10^{16}; 9: 3.2×10^{16}; 10: 1.0×10^{17}; and 11: 3.2×10^{17}.

From 10^{14} cm^{-2} to doses near 10^{17} cm^{-2}, the spectra of the implanted oxides are identical, suggesting that for three orders of magnitude of dose rise the structural damage does not increase. The values of the position and width of the TO_3 band for thermal nonimplanted oxides and for implanted oxides into this saturation regime are given in Table I. Nevertheless, for doses above 10^{17} cm^{-2} (second threshold), other band modifications are observed. Although the position and width of the bands are no longer modified, their intensity and area decrease markedly.

Ellipsometry showed that layer thicknesses were modified after the implantation process. We interpreted the reduction in thickness as a densification and not as a sputtering

TABLE I. Values (in cm^{-1}) for the peak frequency and peak width of the TO_3 band of thermal nonimplanted reference oxides and implanted oxides well into the saturation regime of structural damage.

	Thermal oxide	Implanted oxide
TO_3 frequency (cm^{-1})	1083	1045
TO_3 width (cm^{-1})	78	105

TABLE II. Percentage of decrease in thickness for the higher doses analyzed in this work as measured by ellipsometry.

Dose (cm^{-2})	Thickness decrement (%)
1.0×10^{15}	1.5
1.0×10^{16}	1.5
3.2×10^{16}	1.5
1.0×10^{17}	2.4
3.2×10^{17}	14.2

effect because it increased first for low doses and maintained at a constant value (1.5%) through the three orders of magnitude of dose increment (10^{14}–10^{17} cm^{-2}) at which the regime of damage saturation was extended. However, some dramatic modifications were observed for doses equal to and higher than the second dose threshold previously mentioned (10^{17} cm^{-2}). A major color change in the samples was clearly visible to the naked eye. As deduced from the ellipsometry results, the modifications were due to a marked reduction in thickness and not to a variation of the refractive index. These results are in accordance with the infrared results presented above inasmuch as the evolution of infrared spectra for doses $>10^{17}$ cm^{-2} only consisted of a decrease in the intensity and area of the bands (smaller thickness) but not in position, width, or shape modifications (related with structure). In view of these results, one can conclude that above this second threshold sputtering effects dominate. The percentage reductions in thickness, as measured by ellipsometry, for the higher doses reported in this work, are given in Table II.

B. Annealed samples

All the samples in the range of implantation doses from 10^{13} to 10^{17} cm^{-2} were annealed in a RTA furnace (N_2 atmosphere) at different temperatures from 400 to 1100 °C in order to evaluate the recovery from structural damage after the implantation process. From the infrared spectra it was clearly observed that the modifications of the absorption bands were in the opposite direction with respect to their change following implantation, i.e., the peak frequency of the TO_3 mode shifted toward higher wave numbers, the peak width decreased, and the intensity and area both increased. Nevertheless, the degree of recovery was found to depend on the annealing temperature and on the implantation dose.

For doses below 10^{17} cm^{-2}, the TO_3 peak frequency was restored to that of the original thermal oxide (1083 cm^{-1}) only after annealing at 1100 °C. For doses equal to or above 10^{17} cm^{-2}, the TO_3 band was not restored to the original position. Figure 2 shows the TO_3 peak frequency as a function of implantation dose, for different annealing temperatures. Indeed, for the highest dose shown in Fig. 2 (10^{17} cm^{-2}), the curves deviate from the negative slope characteristic of lower doses, suggesting a different annealing behavior and an incompletely restored structure.

The evolution of the TO_3 peak width with annealing temperature showed a similar pattern (Fig. 3). For doses below 10^{17} cm^{-2} the recovery is important only after annealing at 1100 °C, but there were some difference between the final

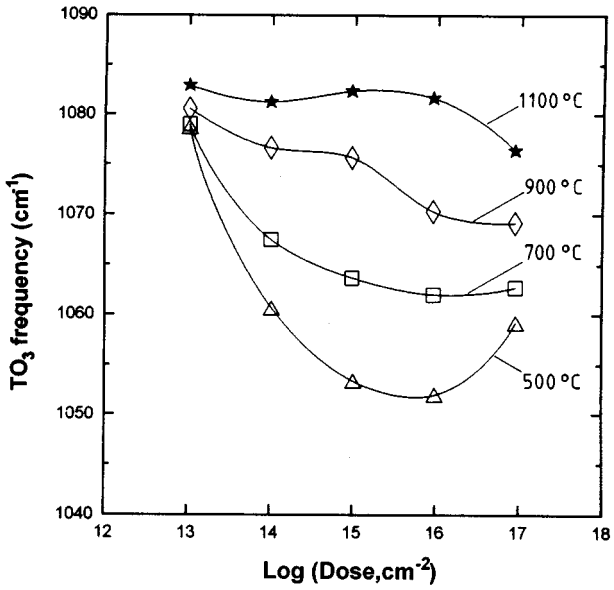

FIG. 2. Peak frequency of the TO_3 band as a function of the implantation dose, for different annealing temperatures. Curves are only a guide for the eye.

value reached after annealing (80 cm^{-1}) and the value of the thermal nonimplanted oxide (78 cm^{-1}). This is consistent with the presence of residual disorder in the structure (wider band) as we discussed below.

IV. ELECTROLUMINESCENCE RESULTS

The EL spectrum for the nonimplanted reference sample is plotted in Fig. 4(a). The most significant result is the presence of a predominant band located at 1.9 eV and a less intense band at 4.3 eV. We examined the 1.9 eV band previously and determined that it was closely related to the sili-

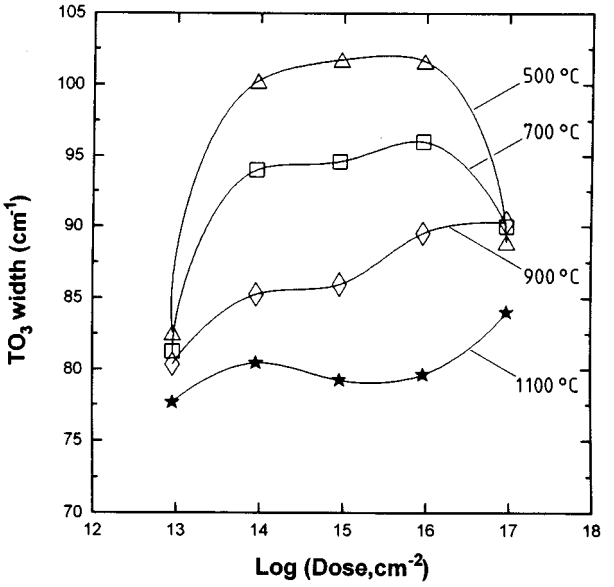

FIG. 3. Peak width of the TO_3 band as a function of the implantation dose, for different annealing temperatures. Curves are only a guide for the eye.

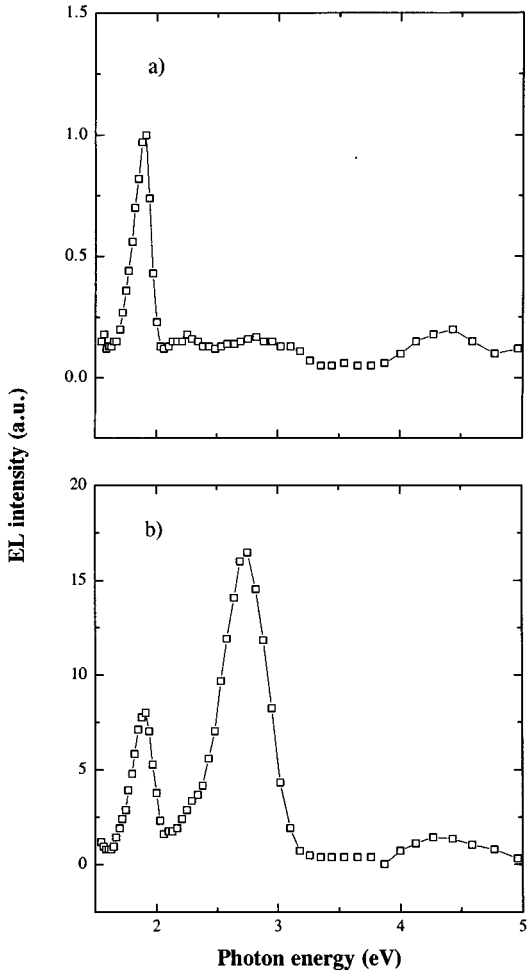

FIG. 4. (a) Electroluminescence spectrum for the nonimplanted structure. (b) Electroluminescence spectrum after implantation at a dose of 1.0×10^{14} cm^{-2}.

con oxidation mechanism.[11] We reported that it is a direct consequence of the wet oxidation process and it is related to the presence of silanol groups, Si–OH, which act as precursors of a negatively charged nonbridging oxygen-hole (NBOH) centers. The band located at 4.3 eV is related to the presence of interface states, as discussed previously.[11] The relatively low intensity of the 4.3 eV band is a consequence of the local distribution of SiO_2/Si interface states.

The Ar ion implantation process produced a marked modification of the previous spectrum. First, a new band located at 2.7 eV appeared, which was accompanied by an increase of the intensity of the 1.9 and 4.3 eV bands [Fig. 4(b)]. The band at 2.7 eV exhibited a significant increase in all the implanted structures. It rose more than two orders of magnitude with respect to the noise level. This band is thought to be a direct consequence of the production of oxygen vacancies by ion implantation. The intensities of the 1.9, 2.7, and 4.3 eV bands increased with the implanted doses for low doses, and showed a tendency to saturate for doses of the order of 10^{14} cm^{-2}. Furthermore, Ar implantation led to an increase of the flatband voltage of the electrolyte–SiO_2–Si system, which is an indication of the presence of a negative charge in the oxide.

As an illustration of the recovery of defects observed after the annealing at 1100 °C, Table III shows the evolution of the three EL bands for the sample implanted with a dose of 1.0×10^{14} cm^{-2}, for different annealing times. Increasing annealing temperature had the same effect as increasing annealing time for a given temperature, although the behavior of each band was different. First, the intensity of the 1.9 eV band decreased after the annealings even to a lower value than before implantation. This result indicates that the recovery of the oxide not only is related to the elimination of defects produced by the implantation but, also, for the decrease of defects, it is present before the implantation. Then, the quality of the initial oxide, at least for this electrically active defect, was improved. Second, a strong decrease in the 2.7 eV band was also observed, but some defects remained even after an annealing at 1100 °C with a duration of 60 s. Finally, we also observed a total recovery of the 4.3 eV band related to the SiO_2/Si interface.

V. DISCUSSION

The structure of amorphous SiO_2 is built up from basic SiO_4 tetrahedral units centered around silicon atoms. However, unlike in the crystalline form, the Si–O–Si intertetrahedral angle of the amorphous material varies from one tetrahedron to another between 120° and 180°.[13,14] The mean value of this Si–O–Si angle distribution is found to be 144°.[15,16] One of the effects of the ion implantation (the same as that found after x-ray or neutron irradiation) is the varied modification of this angle distribution. The densification of the structure found from ellipsometry is a consequence of the Si–O–Si mean angle reduction. Another effect of implantation is to widen the bond angle distribution, and hence increase the dispersion of intertetrahedral angles, which can be regarded as an increment of disorder. These modifications led to shifts and broadenings of the vibrational spectra bands from which compaction and structural disorder could be quantified if no other perturbing effects were modi-

TABLE III. Intensities (in a.u.) of electroluminescence bands. The noise level is located at 1.0×10^3. All the annealed samples were implanted with a dose of 1.0×10^{14} cm^{-2}.

Sample	1.9 eV band	2.7 eV band	4.3 eV band
Nonimplanted	1.0×10^4	···	2.0×10^3
Implanted with 1.0×10^{14} cm^{-2}	8.0×10^4	1.6×10^5	2.0×10^4
1 s annealing (1100 °C)	8.0×10^3	5.3×10^3	4.5×10^3
10 s annealing (1100 °C)	4.5×10^3	2.0×10^3	5.0×10^3
60 s annealing (1100 °C)	2.7×10^3	1.6×10^3	1.5×10^3

fying the bands. Previous experimental studies of silicon oxide implanted with Ar (and other heavy ions) have confirmed some degree of densification.[3,5,6]

However, as well as compaction and disorder, another relevant phenomenon produced after high-dose implantation is the creation of point defects, which arise mainly from broken Si—O bonds and displaced O atoms. In general, it is the presence of these point defects, which are connected with the alteration of the environment of the silicon atom, that is mainly responsible for modifications of the vibrational spectra of implanted samples. This fact can be demonstrated by considering the results of the central force model for SiO_2,[17] in which Si—O—Si bond angle θ and infrared-absorption wave number κ are related by

$$\kappa = \kappa_0 \sin(\theta/2), \tag{1}$$

where $\kappa_0 = 1134\ \mathrm{cm}^{-1}$.[18] The distance between adjacent silicons can be expressed as

$$d_{\mathrm{Si-Si}} = 2r_0 \sin(\theta/2), \tag{2}$$

where r_0 (Si–O distance) takes the value of 1.6 Å. Therefore, as density ρ is inversely proportional to the cube of this distance, an approximate determination of the relative local densification takes the form

$$\frac{\Delta\rho}{\rho_{\mathrm{rel}}} = \left(\frac{\kappa_{\mathrm{rel}}}{\kappa}\right)^3 - 1, \tag{3}$$

where the subscript rel stands for a relaxed oxide. In the same way, we can define the relative strain E in connection with the distance between silicon atoms relative to that of the relaxed oxide. Then, by using Eq. (2), we arrive at

$$E = \frac{\kappa}{\kappa_{\mathrm{rel}}} - 1. \tag{4}$$

Thus, for the 1.5% of densification measured from ellipsometry, the corresponding shift in frequency of the TO_3 mode obtained from Eq. (3) is 5.4 cm^{-1}. Hence, this low degree of densification cannot explain the shifts near 40 cm^{-1} that are measured from infrared spectroscopy (see Table I). Therefore, as expected from the high nuclear damage efficiency of low-energy ion implantation, the most important effects are those connected with point defect creation as a consequence of atom displacement from their equilibrium positions. Another argument is the following: We have shown that the infrared TO_3 mode is at 1083 cm^{-1} for a thermal oxide (nonimplanted), but when oxygen is nonbridging two tetrahedra as a consequence of one broken bond, the value given in the literature for the same stretching vibration is around 1000 cm^{-1},[18] so the infrared band must have a low-frequency contribution, increasing with the implantation dosage, which makes the whole band shift toward lower frequencies.

For doses above the saturation threshold of 10^{14} cm^{-2}, the TO_3 band did not shift to lower wave numbers so we concluded that no further net broken bonds were created. However, we expect the situation is somewhat more complicated because additional implanted ions create defects, but damage is repaired at the same rate as it is produced. We can depict the situation as having oxygen interstitials which diffuse over a sufficient distance before recombining with silicon atoms and hence repairing the previously Si—O broken bonds. For a given oxygen displaced atom this would be easier when the amount of damage is sufficiently high. Nevertheless, ion implantation produces a local increment of temperature of at least some hundreds of degrees within a period of seconds which is probably responsible for the bond restoring equilibrium reached at saturation. This mechanism is valid even after sputtering effects begin to appear because no further net damage is created inside the layer as deduced from the lack of shifts or broadenings of the infrared spectra.

The creation of large numbers of oxygens displaced from their equilibrium positions suggests that a damaged surface layer poor in oxygen must be created. Indeed, surface deviations from bulk concentration are expected to be the result of contamination and oxygen depletion after ion implantation. To corroborate the existence of this layer we performed etching rate measurements in a buffered HF mixture and found that the etching rate increased across the whole range of doses except at higher doses (10^{17} and 3.2×10^{17} cm^{-2}); these samples seemed to remain unetched at the beginning of the experiment. This is consistent with a silicon-rich layer at the surface of implanted samples and the presence of substoichiometric defects. Nevertheless, XPS profiling of the O $1s$ and Si $2p$ atomic levels through the thickness of the layers clearly showed that the composition of the surface SiO_x layer was $x \approx 1.91 \pm 0.03$, whereas the mean value obtained for the bulk was the stoichiometric value 2.01 ± 0.03. Then, although no net mean bulk structural damage is expected after the threshold for saturation (as measured from infrared experiments), increasingly important surface stoichiometric deviation is encountered. For greater implantation doses, a high quantity of oxygen atoms may be sputtered out or displaced deepest in the layer. This behavior explains the reduction in thickness observed.

Nevertheless, the samples implanted with doses above the second threshold of 10^{17} cm^{-2}, showed different annealing behavior. We found that the recovery of the structure was not complete even after the annealing at 1100 °C. As a good illustration, the sample implanted with 3.2×10^{17} cm^{-2} Ar atoms showed a frequency absorption (TO_3 mode) situated at 1045 cm^{-1}. After the annealing at 1100 °C, the position of the band moved to 1075 cm^{-1}, which is far from the thermal oxide peak frequency (1083 cm^{-1}). These results can also be explained by the reduction of thickness and the existence of a surface modified layer poor in oxygen. In fact, the frequency of the TO_3 mode decreases with the thickness of the layer due to optical interference effects.[19] Moreover, following the work of Nakamura, Mochizuki, and Usami,[19,20] who correlated the vibrational response of substoichiometric oxides with their composition, we expect the oxide vibrational band to be shifted from the value of the thermal oxide due to the contribution of the surface SiO_x layer poor in oxygen. Furthermore, added to this previous effects there is the possibility of formation of microcavities for the samples irradiated at very high doses. After the annealing, the Ar trapped in these microcavities evolves, leaving an oxide layer with a certain porosity. Some authors have reported that porous oxide layers present the infrared-absorption band displaced to

TABLE IV. Parameters obtained after the dispersion analysis of implanted oxides. Both TO_3 and TO_4 bands were fitted with two Gaussians each. The parameters indicated are κ_0, frequency of resonance; F, oscillator strength; and σ, dispersion parameter. γ, or damping parameter, which is not indicated, was always approximately equal to 8 cm^{-1} for all the fittings. All the quantities are given in cm^{-1}. (a) Reference samples of SiO_2 nonimplanted; (b) samples implanted with a dose of 10^{15} cm^{-2}; (c) results reported by Naiman *et al.* (see Ref. 22).

	Parameters		Nonimplanted SiO_2 (cm^{-1}) (a)	Implanted SiO_2 (cm^{-1}) (b)	Naiman *et al.* (cm^{-1}) (c)
TO_4	Peak 1	κ_0	1217.9	1218.8	1218
		F	2091.3	1903.6	2200
		σ	35.1	43.8	35
	Peak 2	κ_0	1163.2	1156.3	1164
		F	3118.9	3191.5	3200
		σ	30.3	39.4	30
TO_3 mode	Peak 1	κ_0	1092.1	1061.5	1092
		F	4700.0	5581.5	3900
		σ	11.0	38.5	10.8
	Peak 2	κ_0	1068.5	1034.8	1067
		F	42010.7	35741.4	40100
		σ	29.6	50.2	30.4

lower wave numbers.[21] This is not in contradiction with densification of the whole layer only if local densification is important enough to account for the formation of microcavities. The XPS experiments have shown traces of Ar before annealing and none afterward.

As the infrared response of oxides depends on the amount of absorbing Si—O bonds, we performed approximate calculations of the mean bulk number of Si—O broken bonds as a function of the implantation dose and the annealing temperature. To achieve this we obtained the oscillator strengths and complex dielectric functions of the layers from the frequency dispersion analysis of their transmittance and reflectance spectra. The model for dielectric functions best suited for our purposes here is the one developed by Naiman *et al.*[22] for amorphous materials, which considers that strengths and maximum frequencies of vibrations in amorphous solids are spread in frequency through gaussian shapes. So, each absorption band contributes the following amount to the dielectric function:

$$\Delta\epsilon(\kappa)=\int_0^\infty \frac{4\pi F}{\xi^2-\kappa^2-i\gamma(\xi)\kappa}\, g(\xi-\kappa_0)d\xi, \tag{5}$$

$$g(\xi-\kappa_0)=\frac{1}{\sigma\sqrt{\pi}}\exp-\left(\frac{\xi-\kappa_0}{\sigma}\right)^2, \tag{6}$$

where F is the oscillator strength, κ_0 is the central position of absorption, $\gamma(\xi)=\gamma_0\xi/\kappa_0$ is the oscillator damping, and the function $g(\xi-\kappa_0)$ is a broadening Gaussian curve centered at κ_0 and with σ as full width at half-maximum. The results of dispersion analysis were obtained after fitting the experimental transmittance spectra with Eqs. (5) and (6) and are shown in Table IV. This Table IV include the parameters of the dielectric function obtained for a nonimplanted sample, a sample which has reached damage saturation, and the values reported by Naiman *et al.* for SiO_2.[22] Finally, the number of absorbing Si—O bonds is calculated from

$$N\propto d_{\mathrm{ox}}\int_{\mathrm{band}}\omega\epsilon''(\omega)d\omega, \tag{7}$$

where d_{ox} is the thickness of the oxide and the proportionality constant is obtained from the spectra of the thermal nonimplanted oxide used as reference.

The evolution of the density of broken bonds [broken bonds (N_R)=initial bonds−absorbing bonds detected after implantation] as a function of the implantation dose is shown in a semilogarithmic plot in Fig. 5, relative to the total initial number before implantation. As was previously deduced from the qualitative analysis of the infrared bands, the

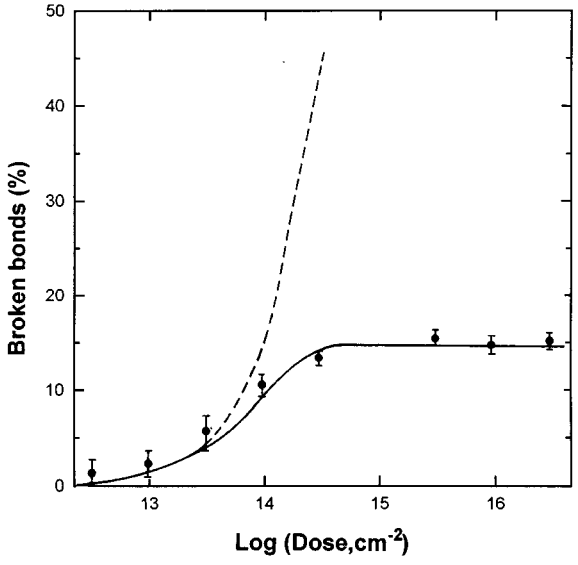

FIG. 5. Number of Si—O broken bonds relative to the initial number of absorbing bonds before implantation, as a function of the implantation dose. The solid line is the theoretical curve fitted to the experimental points. The dashed line is the evolution if damage was proportional to the implanted dose at the initial rate of damage.

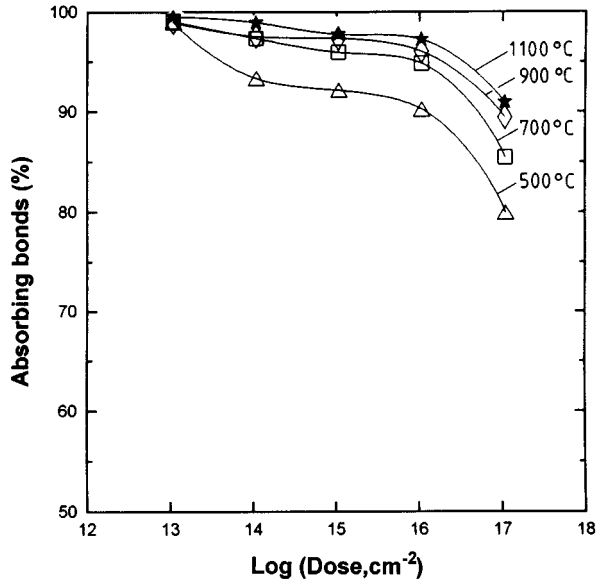

FIG. 6. Number of absorbing bonds relative to the bond density of thermal oxide (taken as 100%) as a function of implantation dose, for different annealing temperatures. Curves are only a guide for the eye.

amount of broken bonds remains constant after a dose of 10^{14} cm^{-2}. We have also represented in Fig. 5 the evolution expected as given by an equation of the type

$$N_R = AN_T(1-e^{-B(D/N_T)}), \tag{8}$$

where D is the implanted dose, N_T is the density of the total initial number of bonds and A and B are constants which were varied during the fitting. This equation is similar to the one obtained if we assume that the process of damage saturation begins as soon as ion tracks overlap for higher doses, similar to the model of thermal and displacement spikes for ion implantation in crystals.[23] After the threshold dose of 10^{17} cm^{-2} (not shown in Fig. 5), the number of absorbing bonds diminishes as a consequence of sputtering, but if thickness corrections are performed, the same amount of damage is observed as in saturation.

In Fig. 6 we have plotted the number of absorbing bonds normalized to the bond density of thermal oxide (taken as 100%) for the different series of annealed samples. The recovery of the broken bonds of the structure is complete even after annealing at 900 °C (electrical defects were observed as being restored from the EL measurements) except for the highest dose for which we expect some oxygen loss from the layer. This behavior clearly means that broken bonds are restored after moderate temperatures. This phenomenon can be understood if we consider that the diffusion coefficient for O into SiO_2 is strongly dependent upon temperature and its value is high at moderate annealing temperatures ($D=2.7\times10^{-4}\ e^{-1.16/kT}$ cm^2/s) so oxygen interstitials can move faster and repair damaged tetrahedra with oxygen vacants.

In contrast, as pointed out above, the peak frequency and peak width of the TO_3 band are only completely recovered for the highest annealing temperature (not significantly for 900 °C). Therefore, for oxide strain relaxation to occur, sufficiently high temperatures and annealing times are needed, so the oxide can flow (viscoelastic relaxation mechanism). For all the results in Figs. 2 and 3 the annealing duration was 10 s, and from the work of Irene, Tierney, and Angiletto *et al.*[24] the viscoelastic relaxation times are: >2 h for 900 °C and 10 s for 1100 °C. From this analysis it is clear that only the annealings performed at the highest temperature were capable of restoring both point defects and distortion and densification of the oxide structure.

TABLE V. Shift in peak frequency in (a) and differences in peak width in (b), between the TO_3 band of a thermal oxide and the layers implanted and annealed. Also given is the relative intrinsic strain in (c) and the local densification in (d) as calculated from the deviations in the peak frequency, following the central force model (see Ref. 17).

Dose (cm^{-2})	Shift in position (a) (cm^{-1})	Difference in width (b) (cm^{-1})	Relative strain (c) (%)	Relative densification (d) (%)
10^{13}	2.2	−2.6	0.20	0.6
10^{14}	6.3	−7.5	0.58	1.7
10^{15}	7.4	−8.2	0.68	2.1
10^{16}	13.0	−11.8	1.20	3.6
10^{17}	14.3	−12.6	1.32	4.0

Therefore, because of the coexistence of two mechanisms of damage—i.e., creation of point defects and distortion-disorder structural modifications—it is difficult to differentiate the two. As the viscoelastic relaxation time is so much greater for an annealing temperature of 900 °C, and with the result that all broken bonds are restored for this annealing time, then, the differences between samples annealed at 900 °C and thermal oxides come about only from distortion induced effects. We give in Table V the difference between peak frequency and width of the TO_3 band for thermal oxides and the oxides implanted and annealed at 900 °C. We also include in this table the relative intrinsic strain and densification values calculated following the central force model for the amorphous SiO_2 [see Eqs. (1)–(4)].[17] The local densification values in saturation are between 2% and 4%, which are slightly higher than the 1.5% densification experimentally obtained from ellipsometry; but, we have to take into account that the values obtained from infrared experiments represent local density values in the neighborhood of a Si—O bond and do not take into account the presence of porosity or microcavities. The more important departures of local densification from measured densification for the higher doses may be explained by the presence of microcavities created by the implanted Ar atoms.

It is very interesting to show how the peak frequency and width of the TO_3 mode evolve together after implantation and annealing. To do so, we show in Fig. 7 the experimental results of peak frequency versus peak width. Several points should be highlighted. The path followed by the implanted samples (damage path) is different from that of the annealing samples (recovering path). The curve for the implanted samples has a higher slope and a significant change occurs near saturation (modification in peak frequency but not in width). Otherwise, the curve for the annealing recovery is smoother and it seems as if peak frequency (related

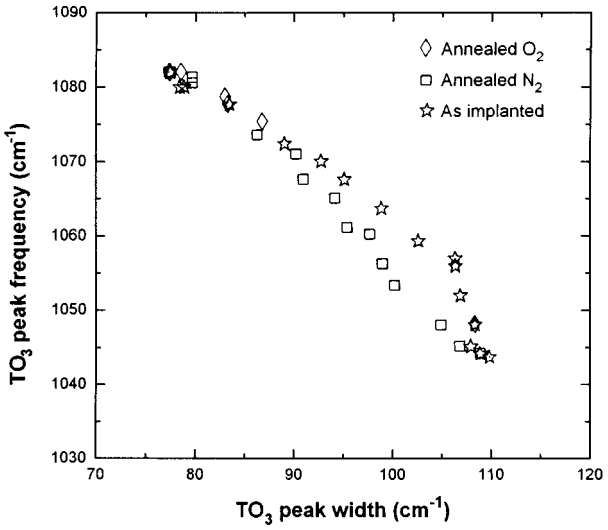

FIG. 7. Peak frequency vs peak width of the TO_3 absorption band for samples implanted and annealed. Additional samples annealed under O_2 atmosphere have been included for comparison.

with strain) and peak width (related with disorder) were similarly recovered. If we subtract two absorbance spectra coming from one as-implanted sample and one annealed sample, both of them with the same value in peak frequency, we can expect the difference (Fig. 8) to be the contribution coming from the nonbridging oxygens because these are the first to be recovered after the annealing (broken bonds are recovered after a 900 °C annealing). We observed a band centered at 990 cm^{-1} which can be associated with the contribution coming from the nonbridging oxygen vibration.

All these results are in agreement with the EL results presented above. The signal coming from all the electrically active defects decreases a point near that of the initial levels. However, some remaining damage may exist, indicated by small differences observed between nonimplanted and annealed samples. These discrepancies become more significant as the implantation dose is raised. Finally, the etching experiments have also shown that samples implanted at high doses ($>10^{16}$ cm^{-2}) and annealed, do not completely recover the structure of the initial nonimplanted oxide because the etching rate obtained is near 150 Å/min, in contrast with the 130 Å/min obtained for a thermal oxide layer. These differences are clearly indicative of a structure which retains point defects and microcavities.

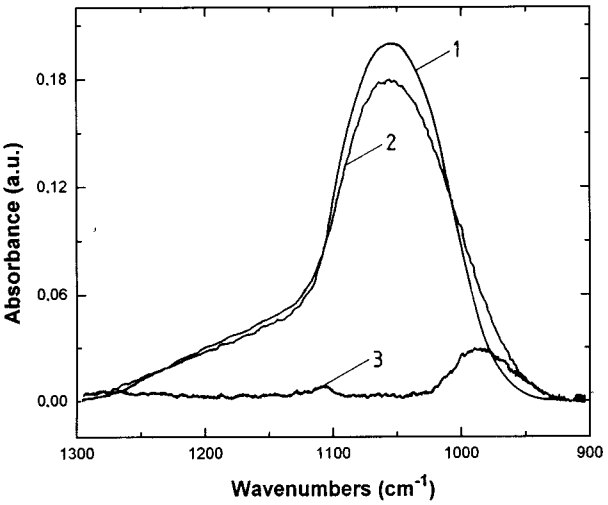

FIG. 8. Substraction of two absorbance spectra coming from one as-implanted sample (1) and another annealed (2) but both of them with the same value for the position of the peak. The difference is a band centered at 990 cm^{-1} (3) which is the contribution of the nonbridging oxygen vibration.

VI. SUMMARY AND CONCLUSIONS

Implantation of low-energy (130 keV) Ar ions in a large range of doses was carried out in thermal silicon oxide layers. The extent of structural damage and its subsequent recovery as a function of the implantation dose and the annealing temperature were characterized by means of ellipsometry, infrared spectroscopy, etching rate measurements, and EL using a new technique based on an EOS system.

Two dose thresholds for damage were encountered: The first at 10^{14} cm^{-2} at which there was a saturation of damage induced by the ion implantation. A dynamic regime was produced at which for high doses damage is repaired at the same rate as it is produced. The second threshold occurs at a dose of 10^{17} cm^{-2}; for doses above this, sputtering dominates.

We have demonstrated the coexistence of two damage mechanisms: Creation of point defects and distortion-disorder structural modifications. From the infrared analysis we were able to separate the effects of several annealed samples and calculated that the local densification in the saturation regime is between 2% and 4%, which is slightly higher than the 1.5% densification obtained by ellipsometry. The presence of microcavities might explain the differences observed.

We have also shown that the evolution of damage during implantation differs from that of recovery during annealing. Annealing led to the smooth recovery of the structure depending on the temperature and duration. Spectral substraction of two samples has shown that the difference between implanted and annealed samples occurs within a small band centered at 990 cm^{-1} originating from the nonbridging oxygen bonds.

The production of a large number of displaced oxygen atoms suggests that a damaged surface layer poor in oxygen is created. Etching rate measurements show that the etching of this surface layer was very slow, consistent with a silicon-rich layer. XPS experiments show a thin surface layer with a composition of $x=1.91$. Therefore, for such highly implanted samples the complete recovery of the structure after annealing is not possible even at the highest temperature (1100 °C).

Annealing at high temperature for a short period has been shown to be effective in restoring the structure of annealed samples. The oxides implanted at moderate doses completely recovered their structure after annealing at 1100 °C, although some disorder remained, as deduced from the vibrational analysis. The viscoelastic relaxation time for this temperature is small enough for the oxides to flow and recover a stressed tetrahedra pattern.

Electrically active defects are nearly completely recovered, as detected by EL, at moderate doses. Nevertheless, annealed sample layers implanted at higher doses ($>10^{16}$ cm^{-2}) do not recover the same etching rate of the original thermal oxide, which is also consistent with the presence of certain substoichiometric defects. This might suggest also the presence of microcavities created by the Ar atoms.

[1] A. Monfret and J. Bernard, in *Ion Implantation in Semiconductors*, edited by I. Ruge and J. Graul (Springer, Berlin, 1971).
[2] A. Hiraiwa, H. Usui, and K. Yagi, Appl. Phys. Lett. **54**, 1106 (1989).
[3] M. C. Busch, A. Slaoui, P. Siffert, E. Dooryhee, and M. Toulemonde, J. Appl. Phys. **71**, 2596 (1992).
[4] R. A. B. Devine, Nucl. Instrum. Methods Phys. Res. B **46**, 244 (1990).
[5] C. Domínguez, B. Garrido, J. Montserrat, J. R. Morante, and J. Samitier, Nucl. Instrum. Methods Phys. Res. B **80/81**, 1367 (1993).
[6] P. Mazzoldi, A. Carnera, F. Caccavale, M. L. Favaro, A. Boscolo-Boscoletto, G. Granozzi, R. Bertoncello, and G. Battaglin, J. Appl. Phys. **70**, 3528 (1991)
[7] B. Garrido, J. Samitier, J. Montserrat, C. Domínguez, and J. R. Morante, Phys. Rev. B **49**, 14 845 (1994).
[8] E. Dooryhee, Y. Langevin, J. Borg, J. P. Duraud, and E. Balanzat, Nucl. Instrum. Methods Phys. Res. B **32**, 264 (1988).
[9] T. P. Ma and P. V. Dressendorfer, *Ionizing Radiation Effects in MOS Devices and Circuits* (Wiley-Interscience, New York, 1989).
[10] D. J. Di Maria, in *The Physics of SiO_2 and its interfaces*, edited by S. T. Pantelides (Pergamon, New York, 1978).
[11] S. Bota, B. Garrido, J. R. Morante, A. Baraban, and P. P. Koronov, Solid-State Electron. (to be published).
[12] A. P. Baraban, P. P. Koronov, S. A. Bota, and J. R. Morante, Mater. Res. Soc. Symp. Proc. **298**, 253 (1993).
[13] C. T. Kirk, Phys. Rev. B **38**, 1255 (1988).
[14] P. Lange, J. Appl. Phys. **66**, 201 (1989).
[15] C. R. Helms, in *The Si–SiO_2 System*, edited by P. Balk (Elsevier, Amsterdam, 1988).
[16] R. L. Mozzi, B. E. Warren, J. Appl. Crystallogr. **2**, 164 (1969).
[17] G. Lucovsky, M. J. Manitini, J. K. Srivastava, and E. A. Irene, J. Vac. Sci. Technol. B **5**, 530 (1987).
[18] T. Furukawa, K. E. Fox, and W. B. White, J. Chem. Phys. **75**, 3226 (1981).
[19] B. Garrido, J. A. Moreno, J. Samitier, and J. R. Morante (unpublished).
[20] M. Nakamura, Y. Mochizuki, and K. Usami, Solid State Commun. **50**, 1079 (1984).
[21] R. M. Almeida and C. G. Pantano, J. Appl. Phys. **68**, 4225 (1990).
[22] M. L. Naiman, C. T. Kirk, B. L. Emerson, J. B. Taitel, and S. Senturia, J. Appl. Phys. **58**, 779 (1985).
[23] F. Seitz and J. S. Koehler, in *Displacements of Atoms During Irradiation*, edited by F. Seitz and D. Turbunbull (Academic, New York, 1956), Vol. 2.
[24] E. A. Irene, E. Tierney, and J. Angilello, J. Electrochem. Soc. **129**, 2594 (1982).